Evaluation of Third Harmonic Component Effects in Five-Phase Synchronous Reluctance Motor Drive Using Time-Stepping Finite-Element Method

Longya Xu, *Senior Member, IEEE,* and Weinong N. Fu

***Abstract*—Interaction of the third harmonic magnetic field with the third harmonic current in a five-phase synchronous reluctance motor (SynRM) can produce additional torque. However, it is still not clear about the SynRM power factor and its impact on the associated power converter because of the third harmonic components. Using time-stepping finite-element method, a mathematical model of the SynRM, which allows any desired harmonic component in computation, is presented. Performance of the five-phase SynRM with two rotor structures has been computed. The study finds that contribution of the third harmonic current to the output torque depends on the rotor structures. It is also shown that the required terminal voltage to regulate the desired current waveform is substantially increased, a result not reported before.**

***Index Terms*—Finite-element methods, synchronous reluctance motor, third harmonic, time stepping.**

I. Introduction

THE synchronous reluctance motor (SynRM) has been favorably used because of the simple rotor structure, high reliability, and low cost. However, the SynRM's poor power/torque density has always ben of great concern. Many types of reluctance rotor structures have been researched to improve the SynRM power/torque density. Another approach to the poor power/torque problem is to add a proper level of third harmonic current to interact with third harmonic magnetic field in the SynRM. The principle and method of adding third harmonic current by using a five-phase stator have been well discussed by the circuit approach [1]–[5]. However, accurate modeling of the SynRM still needs be done to address issues related to optimal electromagnetic design and complete evaluation of the overall system with harmonic excitation, including power converter and controller [1], [2].

As pointed out by recent publications, the SynRM, normally excited with sinusoidal current, now can be excited by a solid-state power converter with any desirable waveforms. It is found that adding proper third harmonic current to the fundamental component to reshape the spatial magnetomotive force (MMF) for a peaked or flat-topped waveform could result in an increased torque-per-ampere ratio. Studies also indicated that, although a three-phase stator winding system cannot support such a desirable third harmonic current circulation, flow of the third harmonic current in a five-phase system is possible. On the other hand, it is still not clear whether injection of third harmonic magnetic field and current may seriously distort the back electromotive force (EMF). It is also not clear whether the required stator terminal voltages to control the current may have to be increased for the desired current shape and the power factor (PF) of the five-phase system may be noticeably reduced, which could lead to an oversized power converter. The literature so far has not addressed the impact of the third harmonic magnetic field and current on the motor and power converter sufficiently.

In this paper, a time-stepping finite-element method (FEM) modeling and evaluation is presented to authentically study the performance of the five-phase SynRM with two typical rotor structures. With the rapidly increased computing power of computers in recent years, accurate modeling of electric machines using FEM has found favor and become a practical tool [6], [7]. With the time-stepping FEM, the desired current waveform can be taken in any shape and the required maintaining voltage be examined. The merits of this method are its straightforward concept and the detailed solution that directly includes the effects of lamination complexity, material saturation, eddy current, rotor movement, and high-order harmonic components of current and magnetic field. Compared to the circuit approach based on conventional d–q transformation and the concept of a matrix of inductance and resistance, the time-stepping field computation mimics the real-time physical operation of the SynRM. Naturally, the results from this method are comprehensive and instructional, not only in terms of internal magnetic field but terminal characteristics. It will be shown in the paper that, indeed, the important effects of nonsine current and magnetic field toward the motor, the associated power converter, and controller are evaluated directly and effectively.

Paper IPCSD 02–002, presented at the 2000 Industry Applications Society Annual Meeting, Rome, Italy, October 8–12, and approved for publication in the IEEE TRANSACTIONS ON INDUSTRY APPLICATIONS by the Electric Machines Committee of the IEEE Industry Applications Society. Manuscript submitted for review May 1, 2000 and released for publication February 19, 2002.

L. Xu is with the Department of Electrical Engineering, The Ohio State University, Columbus, OH 43210-1272 USA (e-mail: xu.12@osu.edu).

W. N. Fu is with Ansoft Corporation, Pittsburgh, PA 15219-1119 USA (e-mail: wfu@ansoft.com).

Publisher Item Identifier S 0093-9994(02)04525-5.

II. SynRM System Description

A. Stator Structure

The stator of the SynRM under investigation consists of a conventional cylindrical structure. It has five phases concentrated, full-pitch windings with wye connection. The five-phase concentrated windings are placed in space in the sequence of A, $-D$, B, $-E$, C from left to right hand. Here, the initial rotor position is as shown in Figs. 1 and 2 (only a quarter of the cross section is shown in both figures). The rotor rotates in

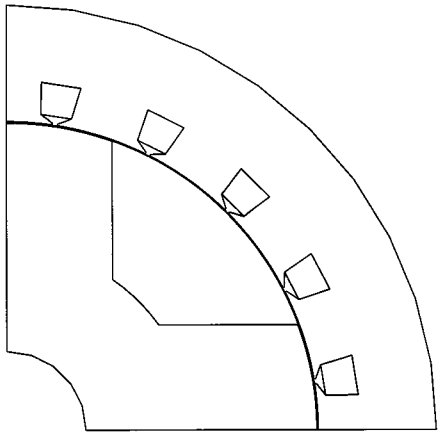

Fig. 1. Structure I (salient-pole rotor).

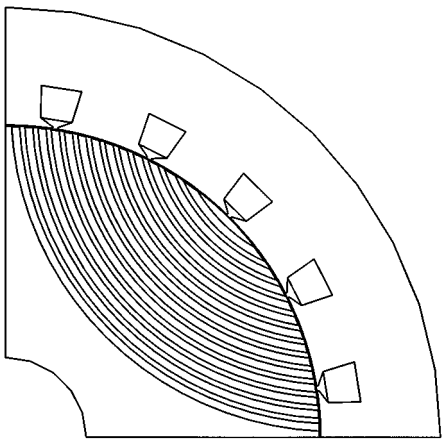

Fig. 2. Structure II (axially laminated rotor).

TABLE I
SPECIFICATIONS OF SynRM

Number of poles	4
Rated stator current (rms)	141.2 A.
Number of turns per slot	7
Rated speed	1800 rpm
Stator diameter	0.421 m
Rotor diameter	0.304 m
Stack length	0.226 m
Air-gap length	0.723×10^{-3} m

the counterclockwise direction. The specification data are listed in Table I.

B. Rotor Structures

Two typical reluctance rotors are investigated in this paper with a common stator. Rotor structure I is as shown in Fig. 1, a traditional salient-pole rotor with simple laminations. The iron core of the rotor is notched out along the q axis to create saliency.

Rotor structure II of the SynRM is an assembly with the axial laminations as shown in Fig. 2.

There are four segments for the four-pole SynRM and the laminations in each segment are interleaved with nonmagnetic materials. Whenever the magnetic flux lines are forced to travel in a path normal to the lamination plane, the flux lines encounter the maximum reluctance. When the flux lines are driven to travel along the lamination plane, the reluctance is minimum [8]. For the rotor studied in this paper, the lamination thickness of Si–Fe plates is 0.38×10^{-3} m and the thickness of the insulation layers 0.25×10^{-3} m.

III. BASIC EQUATIONS OF SynRM

A. Problems Formulation

Since a current-regulated pulsewidth modulation (PWM) voltage-source inverter (VSI) is assumed to provide the controlled current waveforms, the waveform of the stator phase current is known. The objective of computation then is to compute the output torque and stator phase voltage with that the current waveform and the rotor speed are given.

The stator phase currents are expressed as

$$\begin{aligned}
i_A &= \sqrt{2}\left\{I_1\cos(\omega t+\theta_1)+I_3\cos[3\omega t+\theta_3]\right\}\\
i_B &= \sqrt{2}\left\{I_1\cos\left(\omega t+\theta_1-\frac{2\pi}{5}\right)+I_3\cos\left[3\left(\omega t-\frac{2\pi}{5}\right)+\theta_3\right]\right\}\\
i_C &= \sqrt{2}\left\{I_1\cos\left(\omega t+\theta_1-\frac{4\pi}{5}\right)+I_3\cos\left[3\left(\omega t-\frac{4\pi}{5}\right)+\theta_3\right]\right\}\\
i_D &= \sqrt{2}\left\{I_1\cos\left(\omega t+\theta_1+\frac{4\pi}{5}\right)+I_3\cos\left[3\left(\omega t+\frac{4\pi}{5}\right)+\theta_3\right]\right\}\\
i_E &= \sqrt{2}\left\{I_1\cos\left(\omega t+\theta_1+\frac{2\pi}{5}\right)+I_3\cos\left[3\left(\omega t+\frac{2\pi}{5}\right)+\theta_3\right]\right\}
\end{aligned} \tag{1}$$

where the total stator current will be kept at the base value although the ratio of I_3/I_1 may be changed, that is,

$$\sqrt{I_1^2+I_3^2}=Base\ current \quad \text{(rms)}. \tag{2}$$

The following assumptions are made.

- Magnetic field is present only in the plane normal to the machine shaft axis. The magnetic vector potential has an axial component only.
- The B–H curve of iron materials is single valued.
- There are no leakage flux linkages in the outer surface of the stator core and in the inner surface of the rotor core.
- To avoid too many unknowns, for the FEM simulation of the rotor structure II, every ten sheets of laminations and insulation in the rotor are grouped.

In the time-stepping FEM, the field equations for the stator field and the rotor field are written in their own coordinate system. The solutions of the two field equations are matched with each other in the air gap. The FEM mesh of the rotor part is rotated at each time step by an angle corresponding to the mechanical angular frequency [9].

B. FEM Equations

The field equation in the stator iron domain and in the air gap is

$$\nabla\times(\nu\nabla\times A)=0 \tag{3}$$

where A is the axial component of the magnetic vector potential and ν is the reluctivity of the material. In the stator iron core, the eddy current is not considered.

In the stator conductor domain, the field equation is

$$\nabla \times (\nu \nabla \times A) \pm \frac{i_s}{S} = 0 \tag{4}$$

where i_s is the stator phase current and S is the total cross-sectional area of one-turn conductors on one coil side in the FEM model. The "$\pm$" sign becomes "$+$" for the "go" side of the conductor and it becomes "$-$" for the "return" side of the conductor.

The field equation in the rotor iron domain is

$$\nabla \times (\nu \nabla \times A) + \sigma \frac{\partial A}{\partial t} = 0 \tag{5}$$

where σ is the conductivity of the material. In the conventional laminated rotor iron core where the plane of the Si–Fe plate is normal to the axial direction, the second term on the left-hand side is zero.

C. System Equations

Discretizing the field equations (3)–(5) using FEM will give rise to a large system of nonlinear equations [10]

$$[C][A] + [D]\left[\frac{dA}{dt}\right] = [P] \tag{6}$$

where the unknown $[A]$ is the magnetic vector potentials, $[P]$ is the vector associated with input currents, and $[C]$ and $[D]$ are coefficient matrices.

Backward Euler's method is used to discretize the time variable. If the solution at the $(k-1)$th step is known, then at the kth step one has

$$\left[C^k + \frac{D^k}{\Delta t}\right][A^k] = \left[\frac{D^k}{\Delta t}\right][A^{k-1}] + [P^k] \tag{7}$$

where $\Delta t = t^k - t^{k-1}$ is the time step size.

During the time-stepping process, the rotor FEM mesh is moved in accordance with the rotor movement. The Newton–Raphson method coupled with the incomplete Cholesky conjugate gradient algorithm is used to solve (7).

D. Stator Phase Voltage Computation

After solving the equations of FEM, the magnetic field distribution can be obtained. Then, the induced EMF in one stator phase winding is [11]

$$e = \frac{l}{S}\left(\iint_{\Omega^+} \frac{\partial A}{\partial t}\, d\Omega - \iint_{\Omega^-} \frac{\partial A}{\partial t}\, d\Omega\right) \tag{8}$$

where l is the axial length of the iron core, and Ω^+ and Ω^- are, respectively, the cross-sectional areas of the "go" and "return" side of the phase conductors of the coils. Therefore, the stator phase voltage needed is

$$\begin{aligned} v_s &= \frac{l}{S}\left(\iint_{\Omega^+} \frac{\partial A}{\partial t}\, d\Omega - \iint_{\Omega^-} \frac{\partial A}{\partial t}\, d\Omega\right) + R_1 i_s + L_\sigma \frac{di_s}{dt} \\ &= \frac{l}{S}\left(\sum_{i=1}^{N_{\text{element}}} G \frac{A^k - A^{k-1}}{\Delta t} S_i\right) + R_1 i_s + L_\sigma \frac{i_s^k - i_s^{k-1}}{\Delta t} \end{aligned} \tag{9}$$

where R_1 is the total stator resistance of one phase winding, L_σ is the inductance of the end windings, and i_s is stator phase current. N_{element} is the number of elements of one phase, and S_i is the area of element i at the cross-sectional areas of the "go" side of the phase conductors of the coils $G = 1$ and at the "return" side $G = -1$.

E. Torque and PF Computation

The electromagnetic torque can be computed using Maxwell stress tensor method. First, a closed integration circular ring that surrounds the rotor in free space along the air gap must be chosen. Then, the output torque T_e can be obtained by integration along the circular ring [9]

$$T_e = \frac{l}{\mu_0 (r_s - r_r)} \iint_{S_{ag}} r B_r B_\varphi \, dS \tag{10}$$

where r_s and r_r are the outer and inner radii of the circular ring, S_{ag} is the cross-sectional area of the ring, r is the radius varying between the inner and outer radii of the ring with the integration path, and B_r and B_C are the r and C components of the flux density.

Once the SynRM power is computed from the production of torque by rotor angular velocity, the PF can be evaluated by

$$\text{PF} = P_{\text{output}} / 5 v_{\text{rms}} i_{\text{rms}}. \tag{11}$$

F. Mesh Generation and Rotation

The FEM mesh of the cross section of the motor being studied is divided into two parts: the stator and the rotor, with each including a part of the air gap. Meshes of the two parts are then generated separately. Here, the air gap is divided into three layers. Two upper layers belong to the stator and a lower layer belongs to the rotor. Then, the torque can be obtained by integration along the middle layer according to (10). For each part, the mesh is fully automatically generated using the deduction of points algorithm and the mesh refinement method [12].

The unknowns at the innermost nodes of the stator and at the outermost nodes of the rotor are connected by virtue of the "periodic boundary conditions." That is to say, when the rotor is rotated, the shape of the rotor mesh will not be changed, but the coordinates of the rotor mesh and the periodic boundary conditions in the interface of the stator and rotor will. Thus, the stator mesh and the rotor mesh are required to be generated once and only once, and the rotor mesh can be rotated easily.

The results of the generated meshes for studied SynRM are listed below. The solution domain of the FEM is one pole pitch.

Stator:	1816 nodes	and	3297 elements
Rotor I:	1784 nodes	and	3237 elements
Rotor II:	2026 nodes	and	3717 elements.

IV. Computation Results

The proposed time-stepping FEM has been used to simulate the performance of the five-phase SynRM. For the two rotor structures, the output torque and the required stator voltage with and without third current are computed. The time step size is 0.028 ms. Average CPU time for solving the FEM equations at

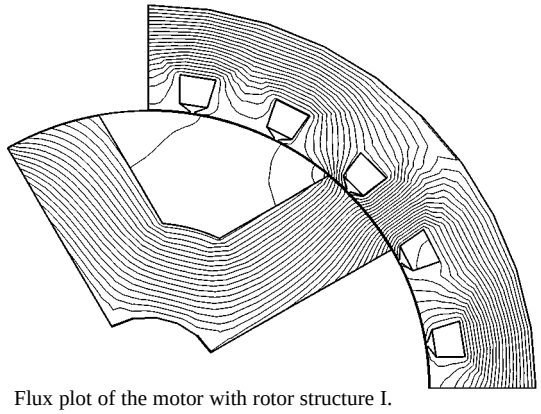

Fig. 3. Flux plot of the motor with rotor structure I.

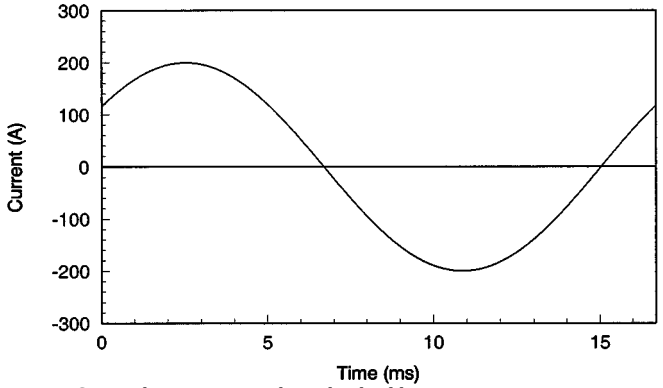

Fig. 4. Stator phase current without the third harmonic current.

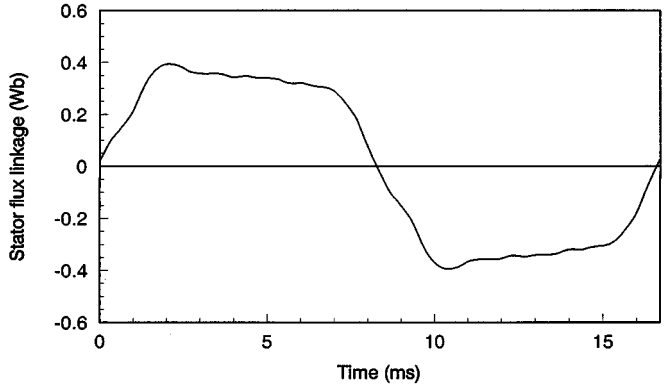

Fig. 5. Computed stator flux linkage without the third harmonic current.

each time step with a Pentium II/366 MHz is about 5 s. In all computed results the angles θ_1 and θ_3 in (1) are optimized so that the maximum output torque is achieved.

A. SynRM With Rotor Structure I

A typical flux plot of the motor with salient-pole rotor on full-load operation is given in Fig. 3. When the third harmonic current is not added (stator current in Fig. 4), the computed stator flux linkage, stator phase voltage, and output torque are shown in Figs. 5–7, respectively.

The computed output torque, stator voltage, and PF of the SynRM, with different amounts of the third harmonic current added, are listed in Table II. It can be seen that, when the third harmonic current is 33.3% of the total current, or the ratio between the fundamental and the third harmonic components is 1 : 0.5, the output torque and motor PF reach the maximum. Both

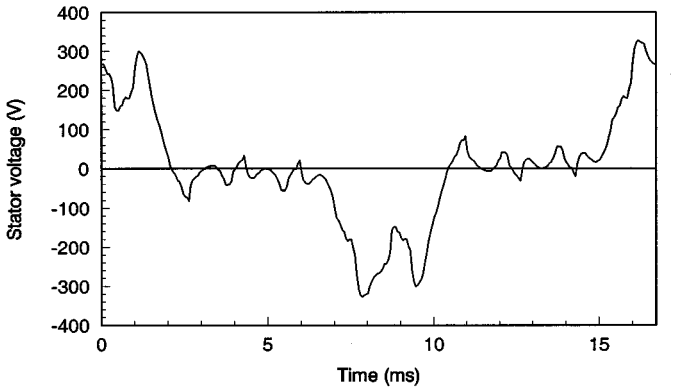

Fig. 6. Computed stator phase voltage without the third harmonic current.

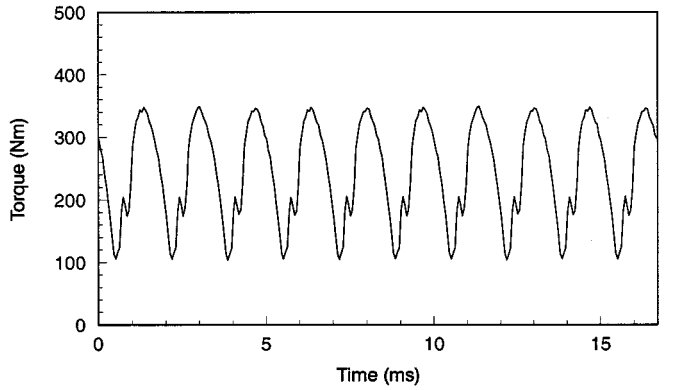

Fig. 7. Computed torque without the third harmonic current.

TABLE II
COMPUTED RESULTS WITH DIFFERENT AMOUNTS OF THIRD HARMONIC CURRENT ADDED (ROTOR STRUCTURE I)

3^{rd} harm.I (%)	Torque (Nm)	V_{rms} (V)	V_{max} (V)	P. F.
0.0	242.7	142.7	329.6	0.45
24.8	290.0	138.5	313.4	0.56
33.3	301.1	132.9	300.2	0.60
37.5	299.6	135.9	310.8	0.59
41.2	290.8	137.5	314.4	0.56

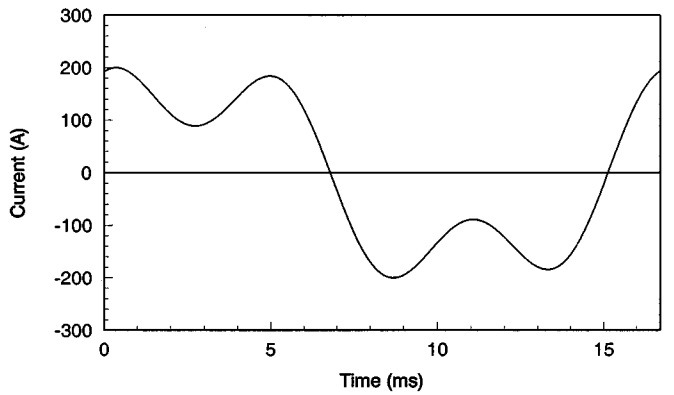

Fig. 8. Stator phase current with 33.3% third harmonic current.

the highest rms and peak voltages do not occur at this level of harmonic current injection, showing the favor of proper utilizing the third harmonic current component. The corresponding stator

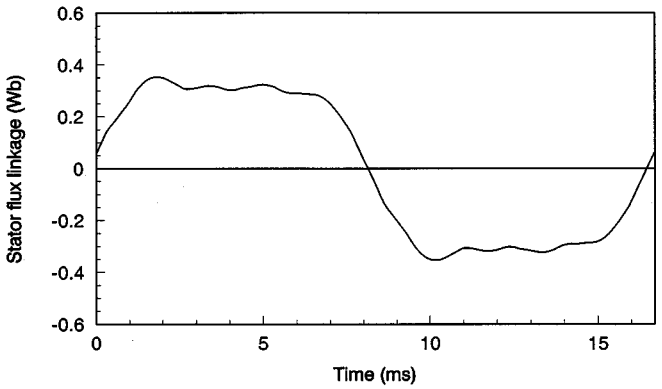

Fig. 9. Computed stator flux linkage with 33.3% third harmonic current.

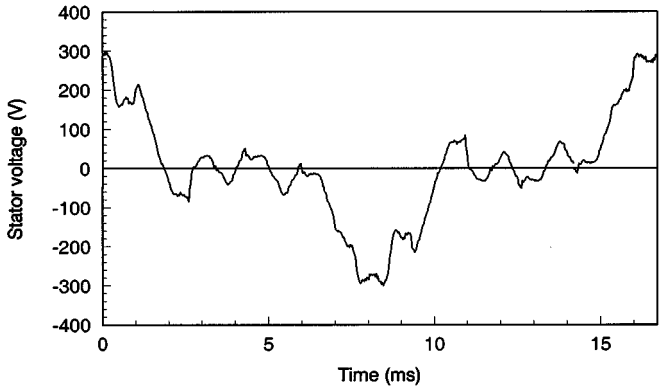

Fig. 10. Computed stator phase voltage with 33.3% third harmonic current.

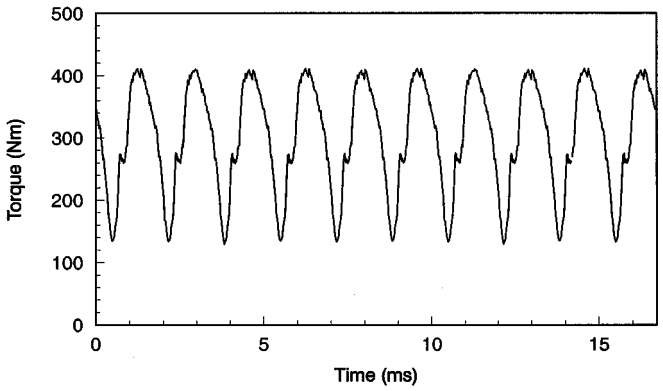

Fig. 11. Computed torque with 33.3% third harmonic current.

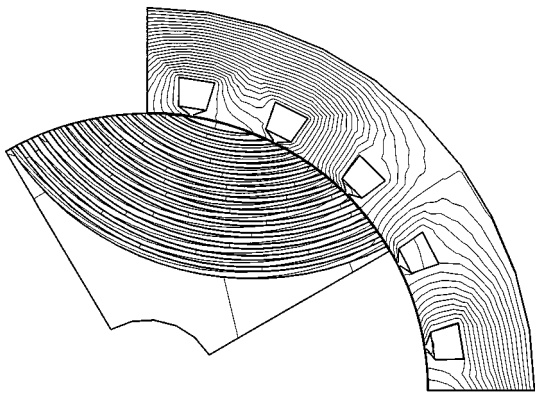

Fig. 12. Flux plot of the motor with structure II.

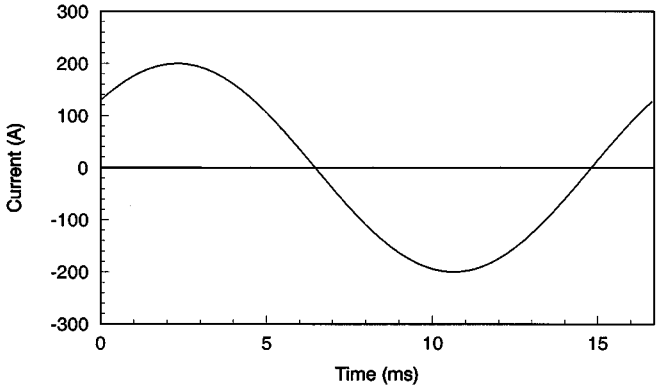

Fig. 13. Stator phase current without the third harmonic current.

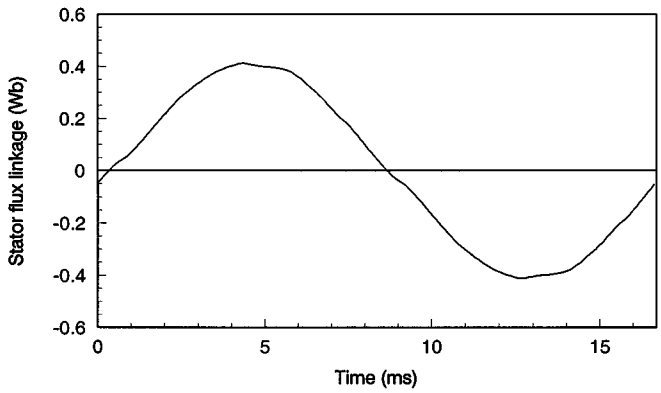

Fig. 14. Computed stator flux linkage without the third harmonic current.

current waveform is shown in Fig. 8 and the computed waveforms of stator flux linkage, stator phase voltage, and output torque in Figs. 9–11, respectively.

However, observing results in Figs. 6 and 10, it is clear that the phase voltage is seriously distorted and contains a large content of third harmonic, regardless of the addition of third harmonic component to the phase current. The peak value of phase voltage reaches 300 V. From Table II, and Figs. 6 and 10, one also can see that when the third harmonic current is added, the peak value of the phase voltage remains almost unchanged. This indicates that the power converter voltage rating can be determined by the operating condition in which pure sine current is assumed.

B. SynRM With Rotor Structure II

A typical flux plot of the motor with the axially laminated rotor on full-load operation is given in Fig. 12. When the third harmonic current is not added (stator phase current is in Fig. 13), the computed stator flux linkage, stator phase voltage, and output torque are shown in Figs. 14–16, respectively.

The computed values of the output torque, stator phase voltage when different amounts of the third harmonic current is added are shown in Table III. It can be seen that when the third harmonic current is added, the output torque, instead of increasing, has been dropped. For the purpose of comparison, when the component of the third harmonic current is 33.3%, the

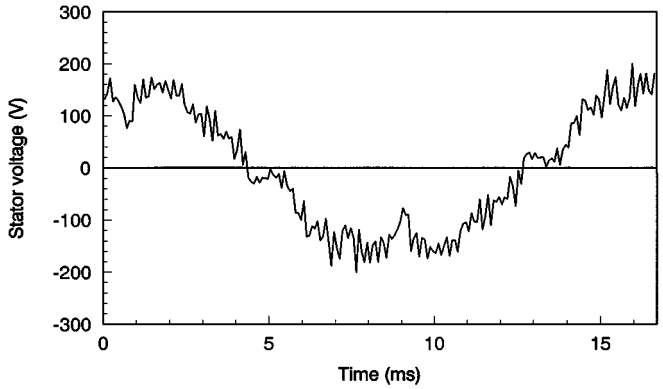

Fig. 15. Computed stator phase voltage without the third harmonic current.

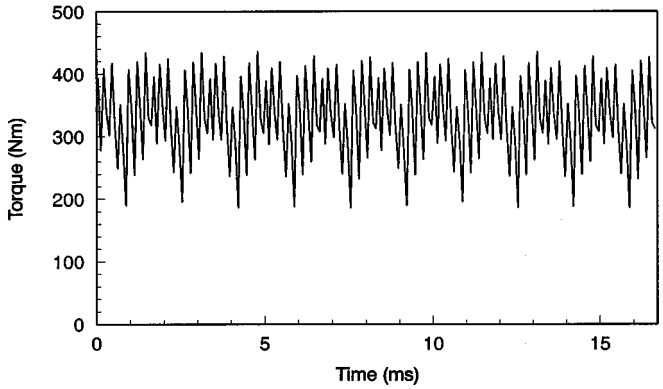

Fig. 16. Computed torque without the third harmonic current.

TABLE III
COMPUTED RESULTS WHEN INPUT DIFFERENT AMOUNTS OF THE THIRD HARMONIC CURRENT (STRUCTURE II)

3rd harm.I (%)	Torque (Nm)	V_{rms} (V)	V_{max} (V)	P. F.
0.0	330.3	115.1	199.9	0.77
24.8	320.2	114.3	186.6	0.75
33.3	311.9	113.8	184.1	0.73
37.5	307.0	113.9	184.2	0.72
41.2	301.8	113.7	182.7	0.71

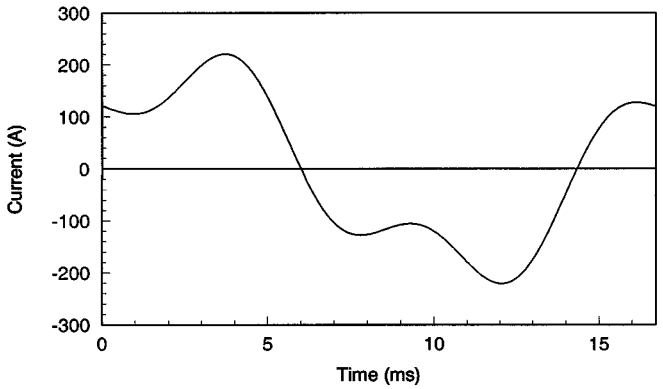

Fig. 17. Stator phase current with 33.3% third harmonic current.

stator phase current waveform is shown in Fig. 17. The computed waveforms of stator flux linkage, stator phase voltage, and output torque are shown in Figs. 18–20, respectively.

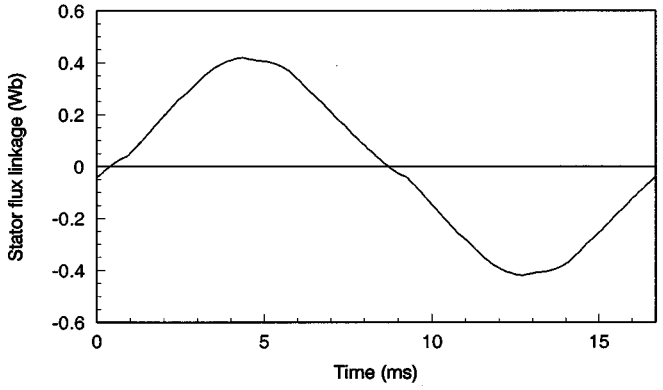

Fig. 18. Computed stator flux linkage with 33.3% third harmonic current.

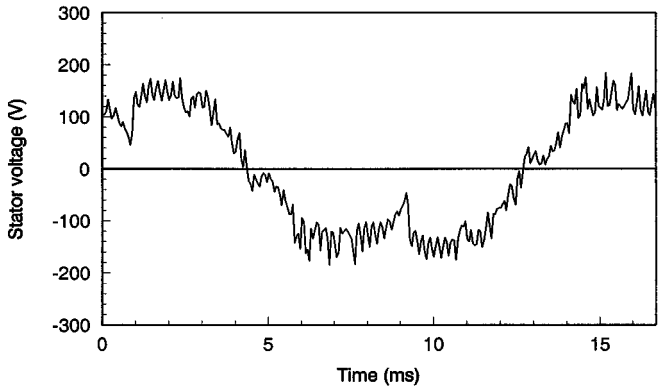

Fig. 19. Computed stator phase voltage with 33.3% third harmonic current.

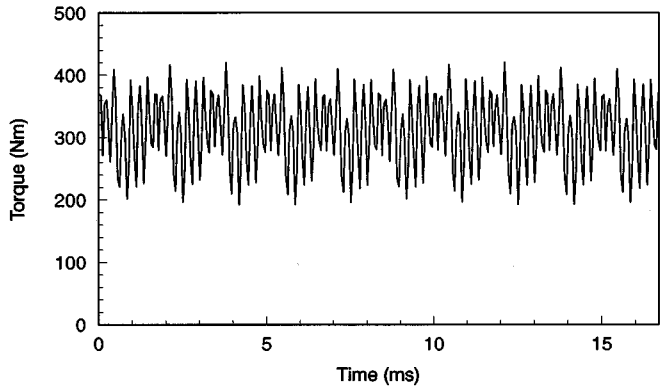

Fig. 20. Computed torque with 33.3% third harmonic current.

The results from Table III clearly indicate that the performance of the SynRM with an axially laminated rotor, including torque production and PF, is much reduced if the three harmonic currents are added into the stator windings.

It can be observed that for the stator flux linkage and phase voltages, the addition of the third harmonic current has minor influence and the waveforms do not change too much and remain largely sinusoidal. The peak value of the required voltage is less than 200 V, substantially lower (184–200 V) than that (315–330 V) for the SynRM with rotor structure I.

V. Conclusions

When one expects to utilize the third harmonic current, interacting with the same order harmonic field in the five-phase SynRM, nonsine waves, both in time and in space, and nonlinear characteristics have significant effects on both the motor and power converter. The proposed time-stepping FEM with rotating meshes is a powerful tool to emulate the operation of the SynRM and directly obtain the various waveforms and determine the power converter ratings. From the results of the time-stepping FEM computation, we can conclude the following.

1) Without third harmonic current added, the output torque of the SynRM with rotor structure II is about 1.4× that with rotor I.
2) If the stator current includes the third harmonic component while keeping the total RMS current unchanged, to the SynRM with rotor structure I, the output torque is increased by about 24%. However, adding third harmonic current content while keeping the total rms current unchanged has a negative increase of torque to the SynRM with rotor structure II.
3) The peak phase voltage of rotor structure I SynRM (330–315 V) is significantly higher than that with rotor structure II (200–184 V). This implies that, to regulate the current to the desired waveform, the associated power converter dc bus has to be rated at least 65% higher than that for the SynRM with rotor structure II.
4) The PF of the SynRM heavily depends on the rotor structure. If the simple salient-pole rotor is used, the PF of the SynRM is quite low due to the undesired harmonic voltage. The PF will improve somewhat if proper third harmonic current is injected to produce useful torque. If the axially laminated rotor is used, the PF of the SynRM improves noticeably. This is because of the much cleaner voltage waveform than that from the SynRM with a simple salient rotor used.
5) From the computed waveform of the torque, one can notice that the main ripple of the torque pulsation has a fixed frequency with respect to the number of the slots of the stator (the frequency is 10 Hz because the number of the stator slots in one pair of poles is ten).

It is apparent that the rotor structure holds a key role in effective utilization of harmonics for useful torque production in the nonsine SynRM. Without considering this dominant rotor role factor, other means, including a five-phase stator winding for circulating three harmonic currents, will not function properly.

References

[1] L. Xu, "Analysis of a doubly-excited brushless reluctance machine by finite element method," in *Conf. Rec. IEEE-IAS Annu. Meeting*, 1992, pp. 171–177.
[2] P. P. Ciufo, D. Platt, and B. S. P. Perera, "Magnetic circuit of a synchronous reluctance motor," in *Electric Machines and Power Systems*. New York: Taylor & Francis, 1999, vol. 27, pp. 253–270.
[3] H. A. Toliyat, L. Xu, and T. A. Lipo, "A five-phase reluctance motor with high specific torque," *IEEE Trans. Ind. Applicat.*, vol. 28, pp. 659–667, May/June 1992.
[4] H. A. Toliyat, S. P. Waikar, and T. A. Lipo, "Analysis and simulation of five-phase synchronous reluctance machines including third harmonic of airgap MMF," *IEEE Trans. Ind. Applicat.*, vol. 34, pp. 332–339, Mar./Apr. 1998.
[5] L. Xu and B. Wang, "Comparison study of rotor structures for five-phase synchronous reluctance machines," in *Conf. Rec. IEEE-IAS Annu. Meeting*, Phoenix, AZ, 1999, pp. 846–853.
[6] L. Xu and E. Ruckstadter, "Direct modeling of switched reluctance machine by coupled field—Circuit method," *IEEE Trans. Energy Conversion*, vol. 10, pp. 446–454, Sept. 1995.
[7] S. L. Ho and W. N. Fu, "Review and further application of finite element methods in induction motors," in *Electric Machines and Power Systems*. New York: Taylor & Francis, 1998, vol. 26, pp. 111–125.
[8] L. Xu, Y. Tang, and L. Ye, "Comparison study of rotor structures of doubly excited brushless reluctance machine by finite element analysis," *IEEE Trans. Energy Conversion*, vol. 9, pp. 165–172, Mar. 1994.
[9] A. Arkkio, "Analysis of induction motors based on the numerical solution of the magnetic field and circuit equations," *Acta Polytech. Scand., Elect. Eng. Ser.*, no. 59, pp. 1–97, 1987.
[10] S. J. Salon, *Finite Element Analysis of Electric Machines*. Norwell, MA: Kluwer, 1995.
[11] S. L. Ho and W. N. Fu, "A comprehensive approach to the solution of direct-coupled multislice model of skewed rotor induction motors using time-stepping eddy-current finite element method," *IEEE Trans. Magn.*, vol. 33, pp. 2265–2273, May 1997.
[12] ——, "A fully automatic mesh generation method for the movement field modeling," in *Proc. 2nd Chinese Int. Conf. Electrical Machines*, Hangzhou, China, Aug. 31–Sept. 2, 1995, pp. 624–630.

Longya Xu (S'89–M'90–SM'93) received the M.S. and Ph.D. degrees in electrical engineering from the University of Wisconsin, Madison, in 1986 and 1990, respectively.

In 1990, he joined the Department of Electrical Engineering, The Ohio State University, Columbus, where he is currently a Professor. He has served as a Consultant to many industrial companies, including Raytheon Company, U.S. Wind Power Company, General Motors, Ford, and Unique Mobility Inc. His research and teaching interests include dynamic modeling and optimized design of electrical machines and power converters for variable-speed generating and drive systems, and application of advanced control theory and digital signal processors in controlling motion systems for super-high-speed operation.

Dr. Xu currently serves as the Chairman of the Electric Machines Committee of the IEEE Industry Applications Society (IAS) and as an Associate Editor of the IEEE Transactions on Power Electronics. He received the 1990 First Prize Paper Award from the IAS Industrial Drives Committee. In 1991, he won a Research Initiation Award from the National Science Foundation. He was also a recipient of the 1995 and 1999 Lumley Research Awards for his research accomplishments from the College of Engineering, The Ohio State University.

Weinong N. Fu was born in Zhejiang, China, in 1961. He received the B.Eng. degree in electrical engineering from Hefei University of Technology, Hefei, China, the M.Eng. degree in electrical engineering from Shanghai University of Technology, Shanghai, China, and the Ph.D. degree from Hong Kong Polytechnic University, Hong Kong, in 1982, 1989, and 1999, respectively.

Following graduation, he joined Shanghai University as a Lecturer. He was a Research Associate at Hong Kong Polytechnic University and a Visiting Researcher in the Data Storage Institute, National University of Singapore, from 1999 to 2001. Since March 2001, he has been an R&D Engineer with Ansoft Corporation, Pittsburgh, PA. He has authored more than 70 papers published in journals and international conference proceedings. His research interests include electromagnetic field computation, motor control and design, and development of novel machines.